

FLOW AND HEAT TRANSFER CHARACTERISTICS AROUND AN ELLIPTIC CYLINDER PLACED IN FRONT OF A CURVED PLATE

by

Mahmoud S. MOSTAFA*, **Radwan KAMAL**, and **Mohamed GOBRAN**

Mechanical Power Department, Faculty of Engineering, Zagazig University, Ash Sharqiyah, Egypt

Original scientific paper
DOI: 10.2298/TSCI120307054M

An experimental investigation has been conducted to clarify heat transfer characteristics and flow behaviors around an elliptic cylinder. Also, flow visualization was carried out to clarify the flow patterns around the cylinder. The elliptic cylinder examined has an axis ratio of 1:2.17, was placed in the focus of a parabolic plate. The test fluid is air and the Reynolds number based on the major axis length, ranged from $5 \cdot 10^3$ to $3 \cdot 10^4$. The angle of attack was changed from 0° to 90° at 15° interval. It is found that the pressure distribution, form drag, location of separation point, and heat transfer coefficient depend strongly upon the angle of attack. Over the Reynolds number range examined, the mean heat transfer coefficient is at its highest at $\alpha = 60^\circ$ - 90° . The values of heat transfer coefficient in the case of free cylinder are higher than those for cylinder/plate combination at all angles of attack and Reynolds number range examined.

Key words: *flow, bluff bodies, forced convection, elliptic cylinder*

Introduction

Flow interaction between bluff bodies has been long investigated for practical and fluid mechanical aspects. Understanding the flow patterns around an interference bodies is useful to explain the heat transfer results around these bodies. For some practical applications a cylinder exists near a solid boundary which affects the flow pattern around the cylinder.

A series of experimental studies upon steady and unsteady flow behaviors of elliptic cylinders have been reported by Modi and Wiland [1], Modi and Dikshit [2, 3] and Modi and Jeong [4]. The mean and fluctuating pressure distributions, the drag, lift, and moment coefficients, the Strouhal number and also the near wake feature were clarified at the subcritical Reynolds number. They described that the Reynolds number range examined was included in the subcritical flow regime and that the aerodynamic characteristics exhibited no dependency upon the Reynolds number. Many authors have investigated flow around an elliptic cylinder at moderate and high Reynolds numbers for a long time.

Many of the drag coefficients obtained have been cited in reference [5]. It can be found that many of the drag coefficients referred by Goldstein [5] decrease steadily with increasing Reynolds number. It suggested that those data were obtained in the critical flow state. The drag

* Corresponding author; e-mail: mmostafa@zu.edu.eg

coefficient and the Strouhal number were measured for an elliptic cylinder of axis ratio 1: 2 at $\alpha = 0^\circ$ and 90° by Delay and Sorensen [6]. The Strouhal number was found to vary discontinuously at the critical Reynolds number. The flow around an elliptic cylinder of axis ratio 1:3 was investigated experimentally in the critical Reynolds number regime by Ota *et al.* [7]. They found that the critical Reynolds number vary with the angle of attack and attains a minimum around $\alpha = 5^\circ$ to 10° . At the critical Reynolds number, the drag, lift, and moment coefficients change discontinuously, and the Strouhal number reaches a maximum of about 1 to 1.5 depending on the angle of attack. Flow around two elliptic cylinders in tandem arrangement was experimentally investigated by Ota and Hideya [8]. They measured the surface static pressure distribution around the elliptic cylinders of axis ratio of 1:3, and found that the flow characteristics vary drastically with the angle of attack and also the cylinder spacing.

Seban and Drake [9] and Drake *et al.*, [10] measured the local heat transfer coefficient on elliptic cylinders of axis ratios 1:4 and 1:3, respectively. The angle of attack examined by them was limited to 0, 5, and 6 degree, and the mean heat transfer coefficient was not measured. Ota *et al.* [11-13] and Ota and Nishiyama [14] studied the effect of cylinder axis ratio, angle of attack, and Reynolds number on the heat transfer coefficient. Also they conducted an experimental investigation to clarify heat transfer characteristics from two and four elliptic cylinders having an axis ratio 1:2 arranged in tandem in a uniform flow of air. They found that the heat transfer features vary drastically with the angle of attack and also with the cylinder spacing. Hanafi *et al.* [15] carried out an experimental investigation to study the effect of plate geometry and gap ratio on the fluid flow and heat transfer characteristics around a heated circular cylinder. The cylinder was placed at various distances of a wall boundary with different geometries (flat or curved plate). They found that the flow patterns and heat transfer characteristics have a strong dependency on the plate geometry and gap ratio. Khan *et al.*, [16] investigated experimentally the cooling process of an array of elliptical tubes of axis ratio 0.3 were placed at zero degree angle of attack. Their results showed that the pressure coefficient across a single tube in the array was remain at approximately 0.16 for $Re > 2 \cdot 10^4$. Both heat transfer rate and Nusslet number were found to vary in power law relationship with Re ; $Nu = 0.26 Re^{0.66}$.

Ibrahim and Gomaa [17] were investigated experimentally and numerically the thermofluid characteristics of the elliptic tube bundle in cross-flow. Their results indicated that increasing the angle of attack clockwise until 90° enhances the convective heat transfer coefficient considerably. The best thermal performance of the elliptic tube bundle was qualified with the lower values of Reynolds number, axis ratio and angle of attack. Faruquee *et al.*, [18] examined numerically the effects of axis ratio on laminar fluid flow around an elliptical cylinder. They found that a pair of steady vortices forms when axis ratio reaches a critical value of 0.34; below this value no vortices are formed behind the elliptical cylinder. The wake size and drag coefficient are found to increase with increase of axis ratio. Johnson *et al.*, [19] examined the effect of axis ratio of elliptic tube on the drag coefficient for axis ratio in the range from 1 (circular cylinder) to ∞ (flat plate normal to the direction of flow). They showed that the drag increases and the critical Reynolds number for the onset of vortex shedding decreases as axis ratio increases. Yoon *et al.*, [20] investigated numerically tow dimensional laminar fluid flow and heat transfer past a circular cylinder near a moving wall. They found that as the gap ratio decreases, the magnitude of lift coefficient for all Reynolds numbers increased significantly with diminishing gap ratio due to the ground effect. As the Reynolds number decreases, the variation of Nusselt number is much significant and increases considerably with decreasing gap ratio.

The purpose of the present study is to investigate the flow and heat transfer characteristics around an elliptic cylinder placed in the focus of a parabolic plate. The elliptic cylinder examined has an axis ratio of 1:217, and the parabolic plate has 90° rim angle and aspect ratio of 1.5. The angle of attack was changed from 0° to 90° at 15° intervals.

Experimental apparatus and technique

Experiments were carried out in two wind tunnels. One of them is used for flow and heat transfer measurements, and the other used for flow visualization. Measurements were conducted in a low speed open circuit wind tunnel discharging air to the atmosphere. The tunnel has a test section area of 0.44 m × 0.44 m and a length of 1.0 m. During the experiments the flow upstream of the cylinder had uniform velocity profile within the range of ±1% of the mean value. The velocity at the entrance of the test section U was measured by means of Pitot tube. The accuracy was about ±0.83%. The experiments were carried out in the subcritical Reynolds number (ranged from $5 \cdot 10^3$ to $3 \cdot 10^4$).

Flow visualization was carried out in a smoke tunnel. The working section of smoke tunnel 0.18 m wide, 0.24 m height, and 0.1 deep, and the flow direction is vertically upwards. In order to obtain a clear picture with more accurate details, the following technique is applied in the present work. A video camera is used to view and record the smoke visualized flow pattern around the model. The video system is connected to a personal computer through a video card. The output video picture is seen on the computer's monitor, and then is captured using spitfire program. This system's unique advantage of variable slow-motion playback, still framing, and slow-motion reverse playback allowed a detailed and clear picture of the flow pattern. The captured flow pattern pictures are then printed later.

Test model

The elliptic cylinder examined was placed in the focus of parabolic plate with rim angle equals 90° (fig. 1). The cylinder has an axis ratio of 1:2.17, the major axis being 27.6 mm and the span wise length 440 mm.

Two cylinders were made of wood and shaped by using an elliptic edge cutter tool with major axis of 28 mm and 14 mm minor axis. One of two cylinders was used for pressure distribution measurement and another was used to measure temperatures distribution around the cylinder surface. Twenty-four longitudinal slots (4 mm depth and 1 mm width) were made at equal intervals on the circumference of the cylinders. The slots start from the mid span of the cylinder to the two ends of it. Stainless steel pipes (0.7 mm outside diameter) were bent from one end at right angle and inserted in these slots. The right angle end of the pipes was inserted perpendicularly on the cylinder surface at the mid span of the cylinder. The other ends of the stainless steel pipes were connected to micro-manometer through rubber tubes to measure pressure distribution around the cylinder surface. Finally the slots were covered with epoxy steel, and the cylinder surface finally was manually finished.

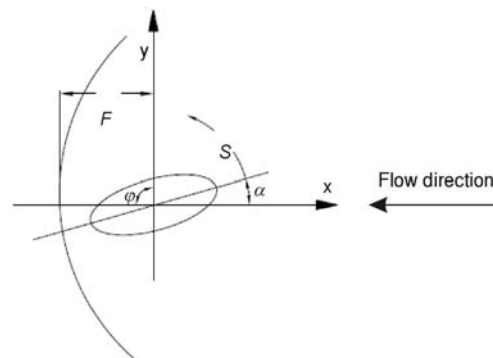


Figure 1. Cylinder/plate combination

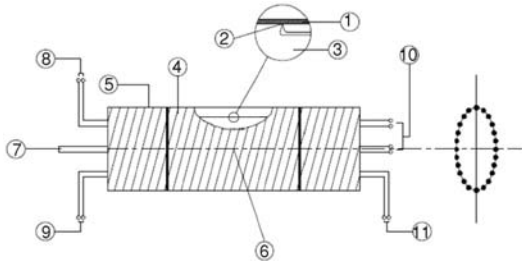


Figure 2. Details of heated cylinder

1 – Nickel chrome foil, 2 – thermocouple junction, 3 – wooden cylinder, 4 – main heater, 5 – guard heater, 6 – pressure tap, 7 – stainless steel tube, 8 – thermocouple leads, 9 – AC power loads for guard heater, 10 – thermocouple leads, 11 – thermocouple leads

Twenty-four copper-constantan thermocouples of 0.4 mm diameter were embedded on the surface of the second cylinder to measure the wall temperature distribution. Finally a nickel-chrome sheet of 0.2 mm thickness and 6 mm width was wound helically and stuck on the cylinder surface. The nickel chrome sheet is divided into three pieces. The mid piece is the active element for the measurements of the local heat transfer. The active element is flanked by two guard pieces, which are used to eliminate the end losses and wall effect (fig. 2). Heating of the cylinder surface was conducted by means of electric current to the nickel chrome sheet under the condition of constant heat flux.

The heat loss by radiation was neglected in the following results. The supplying heat flow rate was determined from the measured power. In operating the system, about one hour was required to attain a steady-state. In the case of a high Reynolds number q was kept at about 1.4 kW/m² but at a low Reynolds number it was decreased to about 0.3 kW/m² in order to minimize the effects of natural convection.

The cylinder was located horizontally at mid height of the test section in the focal plane of the parabolic plate. The surface distance, s , is measured from the leading edge of the cylinder, and it has a positive sign along the suction side and negative sign along the pressure side. The cylinder was located horizontally at mid height of the test section in the focal plan of the parabolic plate.

The parabolic plate was made of plexiglas (120 mm width and 6 mm thickness) with 1.5 aspect ratio. The profile of the parabola can be obtained from the equation:

$$x = \frac{y^2}{4F} \quad (1)$$

$$F = \frac{H}{2 \sin \varphi} (1 + \cos \varphi) \quad (2)$$

where x and y are the co-ordinates of the parabolic plate. The geometrical characteristics of the parabolic plate are $W/C = 6.428$, $H/C = 4.285$, $W/H = 1.5$, $F/C = 2.143$, and $\varphi = 90^\circ$. Figure 1 shows the cylinder-plate combination.

Flow visualization test model

In the present experiments another elliptic cylinder was used to allow flow visualization. The cylinder was made of plexiglas of 100 mm length and 15 mm major axis. Plate used for flow visualization was similar to that used in the experimental measurements.

Flow parameters

In the present study the flow parameters are pressure coefficient (C_p), form drag coefficient (C_D), and lift coefficient (C_L). The pressure distribution was measured by Pitot tube to-

gether with an electronic micro-manometer. The accuracy of the manometer is ± 0.3 mm H₂O. The pressure coefficient at any point along the surface is given as $C_p = (P - P_\infty)/(0.5 \rho U_\infty^2)$. The uncertainty in pressure coefficient is $\pm 2.2\%$. Assuming incompressible flow condition, the dynamic head $0.5 \rho U_\infty^2 = (P_{t_\infty} - P_\infty)$, which can be measured. Finally the pressure coefficient is given by:

$$C_p = (P - P_\infty)/(P_{t_\infty} - P_\infty) \quad (3)$$

The drag and lift coefficients (C_D and C_L) based on the major axis of the elliptic cylinder were evaluated from the pressure distribution by the equations:

$$C_D = \frac{1}{c_s} \int C_p \cos(\beta + \alpha) ds \quad (4)$$

$$C_L = \frac{1}{c_s} \int C_p \sin(\beta + \alpha) ds \quad (5)$$

Integrations were numerically calculated using Simpson-rule. At each point along the cylinder surface (24 points) the angle (β), which is the inclination angle of the pressure vector to the major axis, as shown in fig. 3, was determined (for an axis ratio of 1:2.17) from eq. (6):

$$\beta = \tan^{-1} \left(\frac{4y'}{x'} \right) \quad (6)$$

The position of zero angle of attack was carefully determined by comparing the pressure distributions on two sides of the cylinder. Furthermore, comparisons of the present results (drag and lift coefficients) for cylinder alone with previous data were used to check the validity of measurements. It confirmed a reasonable accuracy of the present elliptic cylinder within $\pm 5\%$.

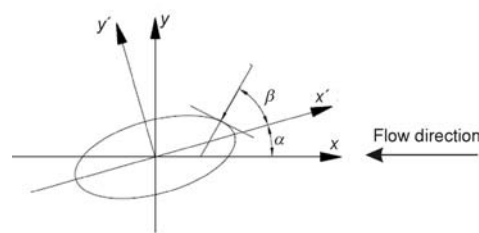


Figure 3. Pressure vector presentation on cylinder surface

Results and discussion

Fluid flow results

Figure 4 illustrates the pressure coefficient distribution along the cylinder surface for cylinder/plate combination compared with that of cylinder alone, at different angle of attacks (0° to 90° at 15° interval).

Figure 4(a) represents the pressure distribution for $\alpha = 0^\circ$. It shows that the pressure distribution vs. the surface distance S/C of the cylinder. The static pressure decreases with increasing distance from the stagnation point until it reaches its minimum value at $S/C = +0.31$ for cylinder alone, and at $S/C = +0.21$ for cylinder/plate combination.

Downstream of these positions, the pressure begins to increase. The boundary layer is no longer able to move against the positive pressure gradient, so it separates from the front part of the cylinder at about $S/C = 0.86$, and -0.86 for cylinder alone and for cylinder/plate combination it separates early at about $S/C = 0.64$, and -0.64 . The separation point was determined by a point at which the static pressure begins to be nearly constant.

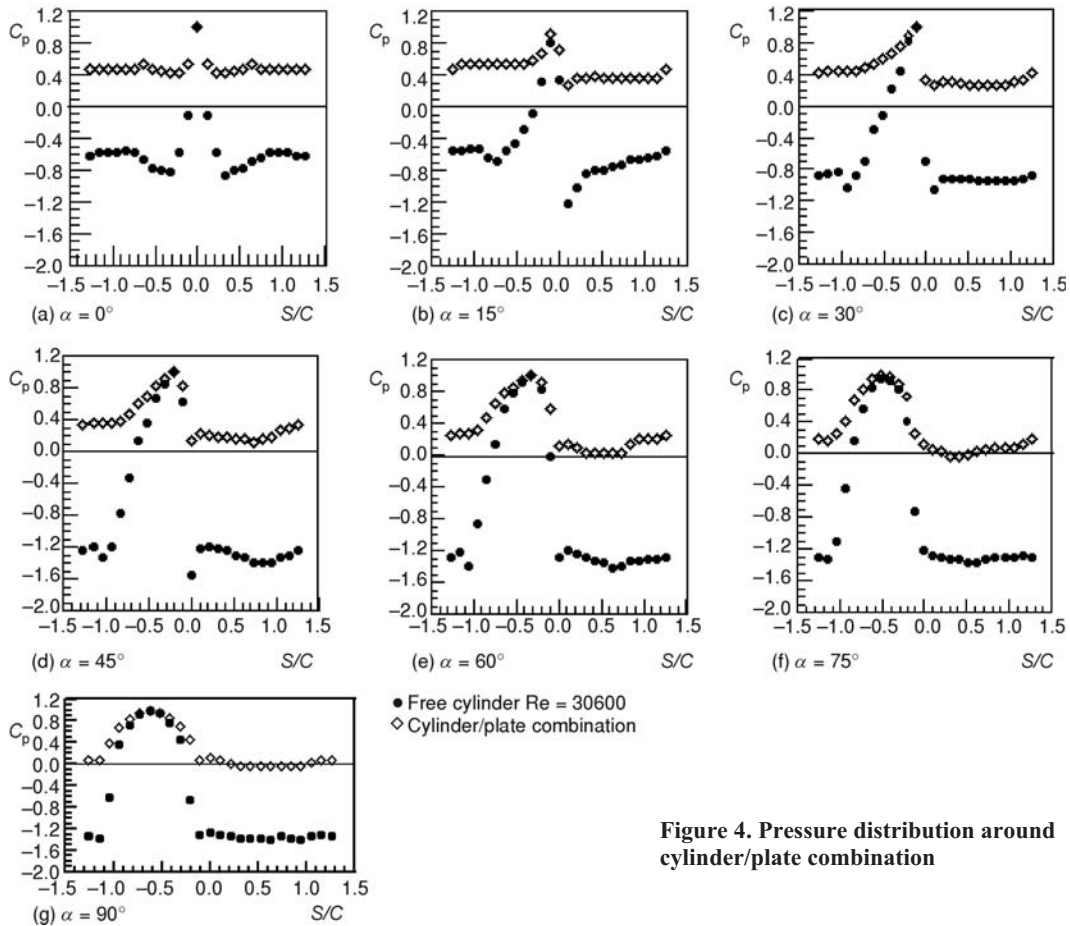


Figure 4. Pressure distribution around cylinder/plate combination

At $\alpha = 15^\circ$, the flow is accelerated very rapidly around the leading edge, producing a very steep decrease of C_p as found in fig. 4(b). The flow on the suction and pressure sides separates at $S/C = 0.3$, and -0.96 , for cylinder alone and at $S/C = 0.2$, and -0.6 , for cylinder/plate combination, respectively.

Figures 4(c) to 4(g) show that, for cylinder/plate combination, the static pressure on the suction side after the separation point is constant till a certain location then, it increases again. The flow on the suction side separates and the separated shear layer reattaches onto the cylinder surface. The location of re-attachment point depends strongly on the angle of attack in the range from 30° to 75° (see fig. 10). This location approaches to the leading edge as the angle of attack increases.

Needless to say, the pressure distribution varies with the angle of attack. This figure reveals that the upstream stagnation point shifts downstream from the leading edge at $\alpha = 0^\circ$ to the minor axis at $\alpha = 90^\circ$. For example it locates at about $S/C = -0.11$ and -0.64 for $\alpha = 15^\circ$ and 90° , respectively. Also it can be seen that, in the case of cylinder/plate combination the values of the static pressure around the cylinder surface are higher than that around the cylinder surface alone.

This can be explained as: when the plate is placed normally in a uniform stream a stagnation region is created on its frontal face, therefore, the flow within the gap between the cylinder and plate becomes nearly stagnant this leads to increase the static pressure on the cylinder surface.

For cylinder/plate combination, at all angles of attack the flow on the pressure side separates early compared with the cylinder alone. It can be detected that at large angles of attack such as 45° and 90° , the location of separation point on the suction side is almost the same as for the single cylinder, and almost coincides with the leading edge.

Finally, one can conclude that the pressure distribution depends strongly upon α . On the suction side, C_p decreases steeply and reaches a minimum, whose location moves upstream with increasing α . On the other hand, the minimum value of C_p on the pressure side moves downstream with an increase of α suggesting a downstream shift of the laminar separation point.

The base pressure coefficient C_{pb} is defined as a value of C_p at the trailing edge of the cylinder. Referring to fig. 5, it is clear that the base pressure depends on the angle of attack. It decreases with increasing the angle of attack. For cylinder/plate combination the base pressure has a higher value compared with the cylinder alone, because the solid boundary of the plate restricts the wake behind the cylinder and the gap between the cylinder and plate is essentially stagnant.

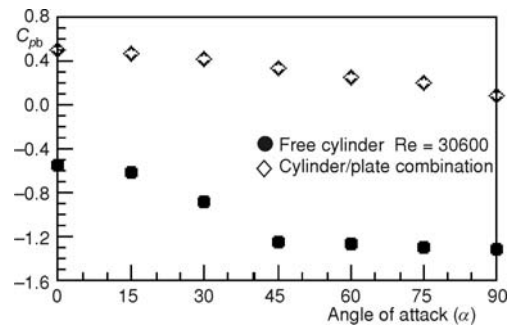


Figure 5. Variation of base pressure coefficient with angle of attack

Figure 6 shows the variation of drag coefficient, C_D , (based on the major axis, c) with α . It can be seen that C_D increases with α from 0.01 to 0.57 when α changed from 0° to 90° for cylinder/plate combination. For all angles of attack the values of form drag for cylinder alone are higher than that of cylinder/plate combination. This is because the gap between the cylinder and plate is essentially stagnant.

Figure 7 shows the variation of the lift coefficient, (C_L) with α . The lift coefficient increases with an increase of α reaching a maximum around $\alpha = 45^\circ$, then decreases. The values of lift coefficient for single cylinder are higher than that for cylinder/plate combination.

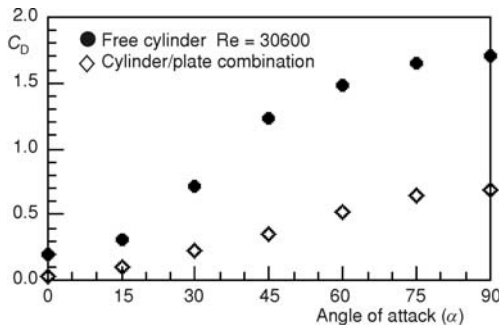


Figure 6. Variation of form drag with angle of attack

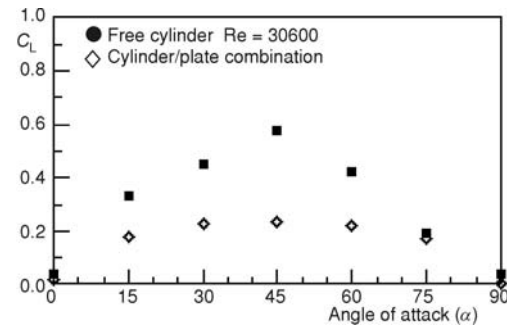


Figure 7. Variation of lift with angle of attack

Figures 8(a) and 8(b) illustrate the variations of the location of separation point on the suction and pressure sides of the cylinder, respectively. For cylinder/plate combination it is clear that the location of separation point shifts to leading edge at $\alpha = 0$ and 15 degree.

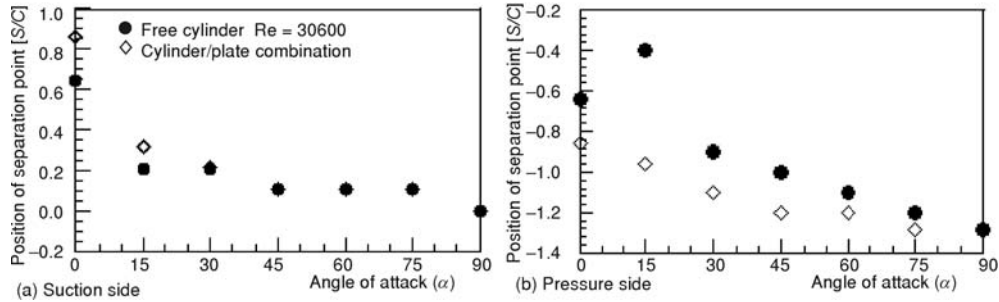


Figure 8. Variation of separation point position on the cylinder surface

Also it can be detected that at large angle of attack such as 45° and 90° , the location of separation point on the suction side fig. 8(a) is almost the same as for the single cylinder, and almost coincides with the leading edge. But on the pressure side, fig. 8(b), the location of separation point approaches to the trailing edge with increasing the angle of attack. Also for cylinder/plate combination the flow on the pressure side separates early compared with that in the case of single cylinder, fig. 10.

Flow visualization

The description of the flow patterns is facilitated with the photographs displayed in figs. 9 and 10. These figures show the flow patterns around the cylinder surface for cylinder alone and cylinder/plate combination, respectively, at different angles of attack. By following

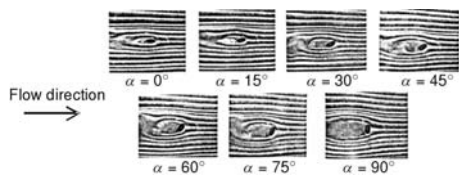


Figure 9. Flow visualization around single cylinder

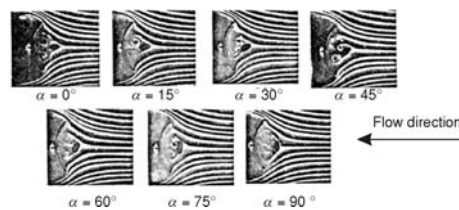


Figure 10. Flow visualization around cylinder/plate combination

the photographs sequence, shown in fig. 9 it is clear that at $\alpha = 0$, a laminar boundary layer developing on the cylinder surface separates from the suction and pressure sides. Consequently a very narrow wake is formed and a vortex street is then formed in the wake of the cylinder. At $\alpha = 15^\circ$, the flow on the suction side separates near the leading edge but it separates near the trailing edge on the pressure side. As angle of attack (α) increases further the position of separation point on the suction side is fixed near the leading edge, although it moves towards the trailing edge on the pressure side. It is clear that the wake width (the wake width is defined as the distance between the separated shear layers behind the cylinder at one minor diameter from the cylinder center) depends strongly upon α , the wake width increases generally with an increase of α .

Figure 10 shows the flow pattern around the cylinder-plate combination. When the plate is placed behind the cylinder, the boundary layer separates from the suction and pressure sides of the cylinder. A pair of unsteady opposite signed vortices with rotational directions is formed. These two vortices are impinging the plate surface and closed re-circulation region forms between the cylinder and plate. Virtually no exchange of fluid occurs between the air in the gap and the free stream. In this sense, the fluid in the gap can be considered to be recirculating but confined stagnant.

Also it is clear that the position of separation point on the suction side of the cylinder is fixed near the leading edge as α increases from 30° to 90° . But on the pressure side it moves towards the trailing edge with increasing α . As α increases from 30° to 75° , the flow on the suction side separates laminarily and the separated shear layer reattaches onto the cylinder surface. The location of re-attachment line depends strongly on the angle of attack in this range. Such location approaches to the leading edge as the angle of attack increases.

Heat transfer results

Local heat transfer

Figure 11 illustrates the local Nusselt number distribution along the cylinder surface for different angles of attack (0 to 90° at 15° interval) at various Reynolds numbers. Also the case of free cylinder is shown. Figure 11(a) represents the local Nusselt number at $\alpha = 0^\circ$. It is clear that the symmetry of the local heat transfer distribution on the upper and lower surfaces is satisfactory at all values of the Reynolds number.

The Nusselt number attains the highest value at the leading edge and decreases steeply with development of a laminar boundary layer on the upstream face. In separated flow region, the Nusselt number again increases in the downstream direction and reaches a maximum at the trailing edge. However, the Nusselt number shows no essential change therein at very low Reynolds number. This may be due to a very stagnant flow in the near wake. At $\alpha = 15^\circ$, the flow is accelerated very rapidly around the leading edge, producing a very steep decrease of the Nusselt number on the upper side compared to the lower side as found in fig. 11(b). It is of interest to note that there exists a region where the Nusselt number shows little change just behind the separation point on the upper and lower sides especially at low Reynolds numbers for cylinder/plate combination.

Figures 11(c) to 11(g) show that, there is unsymmetry of the Nusselt number distribution on the upper and lower sides. It can be seen that with an increase of angle of attack the maximum value of the Nusselt number shifts from the leading edge of the cylinder to a point on the lower surface of the cylinder up to $\alpha = 45^\circ$. This is due to the front stagnation point shift on lower surface of the cylinder with increasing the angle of attack. For $\alpha > 45^\circ$ the maximum value of the Nusselt number occurs on the upper surface of the cylinder in the separated flow region, due to mixing associated with vortex formation in the wake of the cylinder.

Comparing the results at $\alpha = 30^\circ$ and 45° , it can be seen that in the range of $\alpha > 30^\circ$ the heat transfer coefficient in the separated flow region is larger than that on the upstream surface where the boundary layer develops. This may be due to the fact that the wake width behind the cylinder increases with the angle of attack.

Needless to say, the local heat transfer coefficient distribution varies with the angle of attack. Figure 11 reveals that increasing the angle of attack the maximum value of the Nusselt number shifts from the leading edge. Also it can be seen that, in the case of cylinder/plate combi-

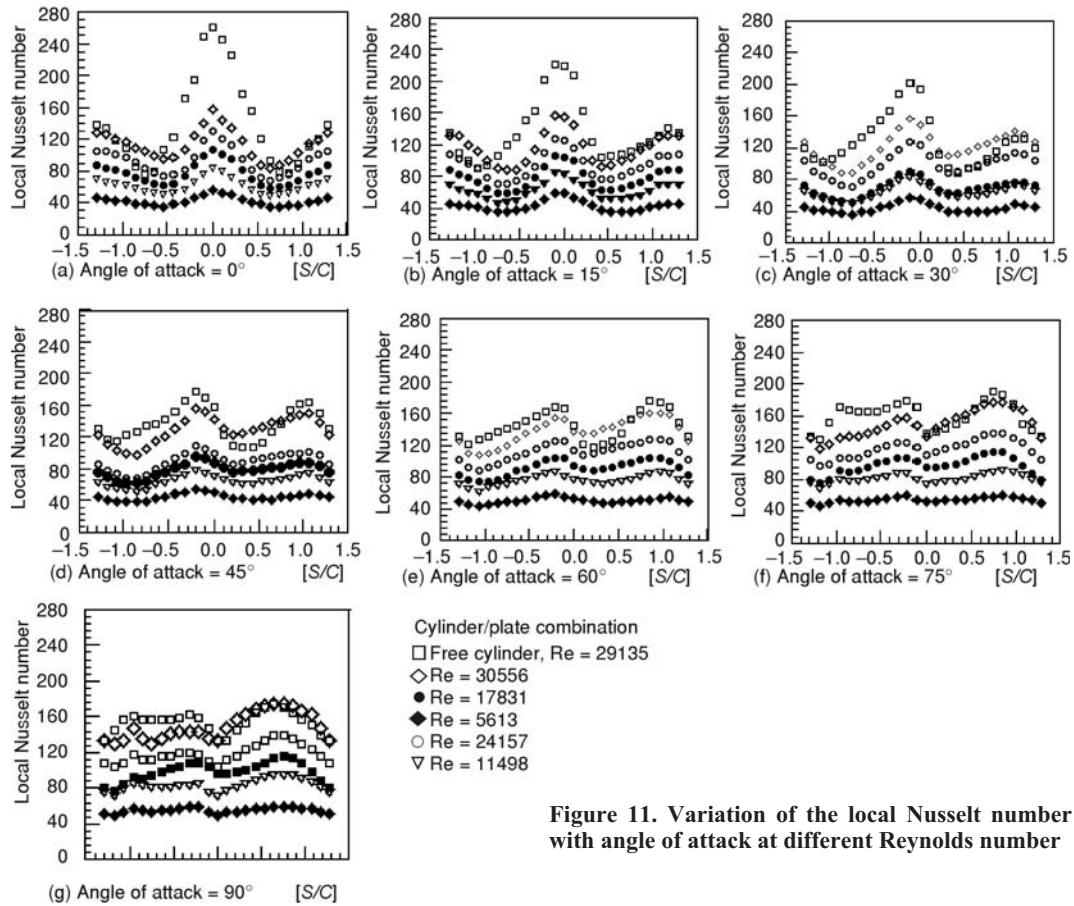


Figure 11. Variation of the local Nusselt number with angle of attack at different Reynolds number

nation the values of local heat transfer coefficient around the cylinder surface are smaller than those around the cylinder surface alone at all Reynolds numbers. This can be explained as follows: when the plate is placed normally in a uniform stream a stagnation region is created on its frontal face. Therefore, the flow within the gap between the cylinder and plate becomes nearly stagnant. This leads to a decrease in the heat transfer coefficient.

Mean heat transfer

The mean Nusselt number, Nu_m , over the whole circumference of the elliptic cylinder was estimated by using numerical integration. The mean Nusselt number is calculated from the following equation:

$$Nu_m = \frac{h_m c}{k} \quad (7)$$

$$h_m = \frac{1}{B} \int_0^B h ds \quad (8)$$

Figure 12 illustrates the variation of Nu_m with α . It can be seen that in the low Reynolds number range of about $Re < 11300$ for single cylinder and $Re < 24100$ for cylin-

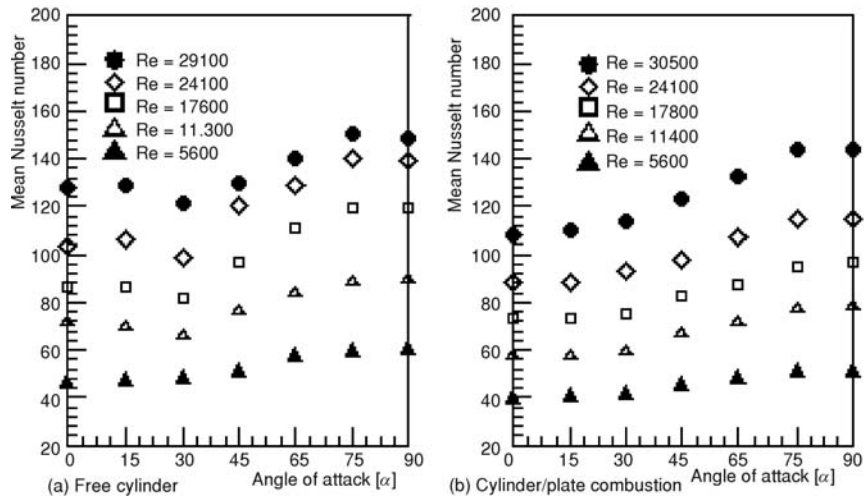


Figure 12. Variation of mean Nusselt number with angle of attack

der/plate combination, no essential change in the region of $\alpha = 0^\circ$ to 30° . Beyond $\alpha = 30^\circ$, Nu_m increases slightly with α . On the other hand, in the region of $Re \geq 11300$ for single cylinder Nu_m decreases with α in $0 < \alpha < 30^\circ$, reaching a minimum around $\alpha = 30^\circ$, and subsequently increases with α . The mean heat transfer coefficient attains a maximum at α in the range $75^\circ \leq \alpha \leq 90^\circ$ for all values of Reynolds number studied.

For cylinder/plate combination in the region $Re \geq 24100$ Nu_m increases with a . Figure 13 shows the variation of Nu_m with Reynolds number at $\alpha = 0$. It can be seen that the values of Nu_m for free cylinder are in a good agreement with Ota work [5]. Also the values of mean Nusselt number for cylinder/plate combination are lower than those of free cylinder by about 15%. This is due to the stagnation region in the gap between the cylinder and plate.

The relation between mean Nusselt number and Reynolds number for all angles of attack is presented in fig. 14 for cylinder/plate combination. It is clear that as the Reynolds number

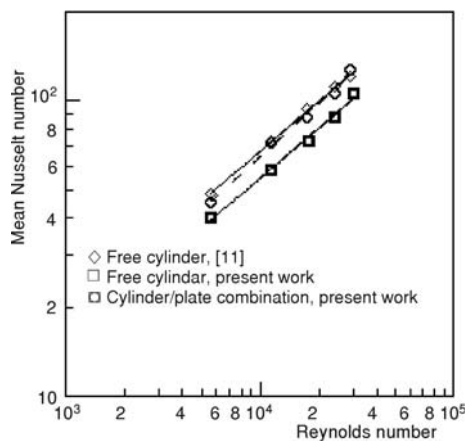


Figure 13. Mean Nusselt number at $\alpha = 0^\circ$

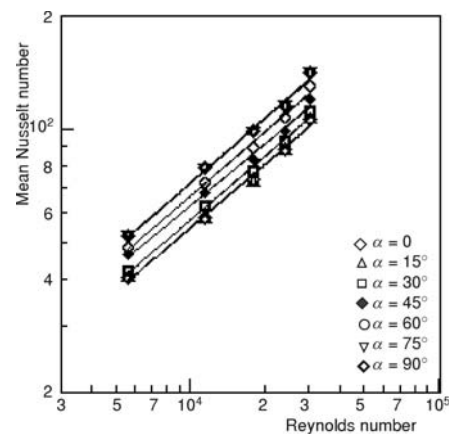


Figure 14. Effect of angle of attack on mean Nusselt number for cylinder/plate combination

increases the value of Nu_m increases for all angles of attack. This is due to the decrease in the boundary layer thickness in the leading edge zone, and strong mixing of fluid in the separated region. It can be seen that as the angle of attack increases in the range $30^\circ \leq \alpha \leq 60^\circ$ the value of Nu_m increases. This is due to increase the wake width in the separated region [10]. At $\alpha = 0^\circ$ and 15° , and at $\alpha = 75^\circ$ and 90° the values of Nu_m are identical at all Reynolds numbers.

Correlation between the mean Nusselt number and angles of attack

Table 2. values of a , m , and n

	a	m	N
Free cylinder	0.452	0.571	0.254
Cylinder/plate combination	0.339	0.584	0.246

It is clear that the mean Nusselt number depends on the Reynolds number and angles of attack. A trial is made to correlate these parameters and a general empirical formula is obtained in the form:

$$Nu_m = aRe^m[1 - n \cos\alpha] \quad (9)$$

The values a , m , and n are listed in tab. 2 for single elliptic cylinder and cylinder/plate combination.

Figure 15 shows a comparison between the experimental results and those calculated from the empirical equation. It can be seen that the experimental results are in a good agreement with those calculated from the empirical eq. 5 within 11.8% for free cylinder and 8.5% for cylinder/plate combination (maximum percentage error).

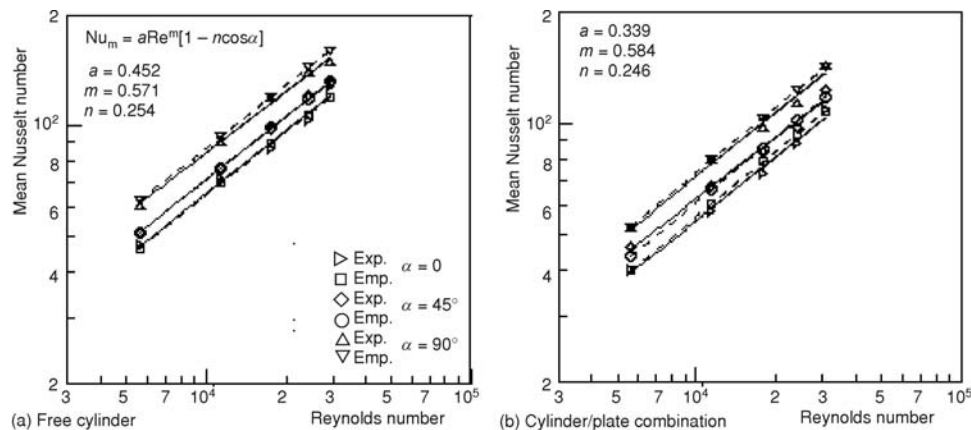


Figure 15. Correlation of mean Nusselt number with Reynolds number as a function of angle of attack

Concluding remarks

The effect of parabolic plate on the flow characteristics around an elliptic cylinder was experimentally investigated at $Re = 3 \cdot 10^4$. It has been found that the pressure distribution depends strongly upon α . On the suction side ($s/c > 0$), C_p decreases steeply and reaches a minimum, whose location moves upstream with increasing α . On the other hand, the minimum value of C_p on the pressure side moves downstream with an increase of α . For cylinder/plate combina-

tion the form drag increases with α but its values are lower than that of single cylinder. The location of separation point on the suction side shifts to leading edge at $\alpha = 0$ and 15° compared with that in the case of single cylinder. Also as the angle of attack increases the flow on the pressure side separates early than that of single cylinder. The wake width depends strongly upon α , the wake width increases generally with an increase of α . The position of separation point on the suction side of the cylinder is fixed near the leading edge as α increases from 30° to 90° . But on the pressure side it moves towards the trailing edge with increasing α . For cylinder-plate combination as α increases from 30° to 75° , the flow on the suction side separates laminarily and the separated shear layer re-attaches onto the cylinder surface. The location of re-attachment point depends strongly on the angle of attack in this range. When the plate is placed behind the cylinder, a pair of large unsteady opposite signed vortices or eddies with rotational directions are formed. The fluid in the gap can be considered to be re-circulating but stagnant.

Heat transfer characteristics of an elliptic cylinder having an axis ratio 1:2.17 and cylinder/plate combination are clarified through wind tunnel experiments. The Reynolds number range examined is from about $5.5 \cdot 10^3$ to $3 \cdot 10^4$ and the angle of attack is varied from 0 to 90° . It has been found that:

- the local heat transfer features of free cylinder are, in general, independent of the Reynolds number, and are different from those of a cylinder/plate combination,
- the dependency of the mean heat transfer coefficient upon the Reynolds number and angle of attack is clearly recognized; over the Reynolds number range examined the values of Nu_m at $\alpha = 75^\circ$ and 90° are nearly equal to each other and are the highest; for free cylinder, Nu_m is lowest at $\alpha = 30^\circ$ but for cylinder/plate combination, Nu_m is lowest at $\alpha = 0$; no essential change in the values of Nu_m is observed in the range of $0 \leq \alpha \leq 15^\circ$,
- the values of Nu_m for free cylinder are higher than that for cylinder/plate combination at all angles of attack and Reynolds number range examined,
- the value of mean Nusselt number for free cylinder and cylinder/plate combination can be calculated from the following equation: $Nu_m = aRe^m[1 - n \cos\alpha]$ with maximum percentage error $\pm 11.8\%$ for free cylinder and $\pm 8.5\%$ for cylinder/plate combination.

Nomenclature

C	– major axis of elliptic cylinder	q	– heat flux, [Wm^{-2}]
C_D	– drag coefficient, ($= D/0.5\rho U_\infty^2 c$)	U_∞	– free stream velocity, [ms^{-1}]
C_L	– lift coefficient, ($= L/0.5\rho U_\infty^2 c$)	Re	– Reynolds number ($= \rho U_\infty c/\mu$)
C_p	– pressure coefficient, [$= (P - P_0)/0.5\rho U_\infty^2 c$]	r	– position vector
C_{pb}	– base pressure coefficient	S	– surface distance from leading edge, [m]
D	– drag, force per unit length, [Nm^{-1}]	W	– parabolic plate width, [m]
F	– focal length, [m]	x, y	– general co-ordinates
H	– height of parabolic plate, [m]	x', y'	– ellipse co-ordinate
h	– heat transfer coefficient, [$Wm^{-2}C$]	<i>Greek symbols</i>	
h_m	– mean heat transfer coefficient, [$Wm^{-2}C^{-1}$]	α	– angle of attack, [deg.]
k	– thermal conductivity, [$Wm^{-1}C^{-1}$]	β	– pressure-x axis angle, [deg]
L	– lift, force per unit length, [Nm^{-1}]	θ	– co-ordinate angle, [deg.]
Nu	– local Nusselt number ($= hc/k$)	φ	– rim angle
Nu_m	– mean Nusselt number ($= h_m c/k$)	μ	– free stream dynamic viscosity, [Nsm^{-2}]
P_∞	– free stream static pressure, [Nm^{-2}]	ρ	– free stream density, [kgm^{-3}]
$P_{t\infty}$	– total free stream pressure, [Nm^{-2}]		

References

- [1] Modi, V. J., Wiland, E., Unsteady Aerodynamics of Stationally Elliptic Cylinders in Subcritical Flow, *AIAA J.*, 8 (1970), 10, pp. 1814-1821
- [2] Modi, V. J., Dikshit, A. K., Mean Aerodynamics of Stationally Elliptic Cylinders in Subcritical Flow, *Proceedings*, Thrid International Conference on Wind Effects on Buildings and Structures, Tokyo, 1979, pp. 345-355
- [3] Modi, V. J., Dikshit, A. K., Near-Wakes of Elliptic Cylinders in Subcritical Flow, *AIAA J.*, 13 (1975), 4, pp. 490-497
- [4] Modi, V. J., Jeong, L., On Some Aspects of Unsteady Aerodynamics and Vortex Induced Oscillations of Elliptic Cylinders at Subcritical Reynolds Number, *ASME Journal of Mechanical Design*, 100 (1978), 2, pp. 354-362.
- [5] ***, *Modern Developments in Fluid Dynamic* (Ed. S. Goldstein), Vol. II, Oxford Univ. press, UK, 1938
- [6] Delay, N. K., Sorensen, N. E., Low-Speed Drag of Cylinders of Various Shapes, NACA Tech. Note, no. 3038, 1953
- [7] Ota, T., et al., Flow Around an Elliptic Cylinder in the Critical Reynolds Number Regime, *Journal of Fluids Engineering*, 109 (1987), 2, pp 149-155
- [8] Ota, T., Hideya, N., Flow Around Two Elliptic Cylinders in Tandem Arrangement, *Journal of Fluids Engineering*, 108 (1986), 1, pp. 98-103
- [9] Seban, R. A., Drake, R. M., Local Heat Transfer Coefficients on the Surface of an Elliptic Cylinder in a High Speed air Flow, *Trans. ASME*, 75 (1953), pp. 235-240
- [10] Drake, R. M., et al., Local Heat Transfer Coefficient on Surface of an Elliptic Cylinder, Axis Ratio 1:3, in a High Speed Air Flow, *Trans. ASME*, 75 (1953), pp. 1291-1302
- [11] Ota, T., et al., Forced Convection Heat Transfer from an Elliptic Cylinder of Axis Ratio 1:2, *Bull JSME*, 26 (1983), pp. 262-267
- [12] Ota, T., et al., Heat Transfer and Flow Around an Elliptic Cylinder, *Int. J. Heat Mass Transfer*, 27 (1984), 10, pp. 1771-1779
- [13] Ota, T., et al., Heat Transfer From Two Elliptic Cylinders in Tandem Arrangement, *Trans. ASME, J. Heat Transfer*, 108 (1986), 3, pp. 252-531
- [14] Ota, T., Nishiyama, H., Flow Around Two Elliptic Cylinders in Tandem Arrangement, *Trans. ASME, J. Fluid Eng.*, 108 (1986), 1, pp. 98-103
- [15] Hanafi, A. S., et al., Fluid Flow and Heat Transfer Around Circular Cylinder-Flat and Curved Plates Combinations, *Experimental Thermal and Fluid Science*, 25 (2002), 8, pp. 631-649
- [16] Khan, M. G., et al., An Experimental Characterization of Cross-Flow Cooling of Air Via An In-Line Elliptical Tube Array, *International Journal of Heat and Fluid Flow*, 25 (2004), 4, pp. 636-648
- [17] Ibrahim, T. A., Gomaa, A., Thermal Performance Criteria of Elliptic Tube Bundle in Cross Flow, *International Journal of Thermal Science*, 48 (2009), 11, pp. 2148-2158
- [18] Faruque, Z., et al., The Effect of Axis Ratio on Laminar Fluid Flow Around an Elliptical Cylinder, *International Journal of Heat and Fluid Flow*, 28 (2007), 5, pp. 1178-1189
- [19] Johnson, S. A., et al., Predicted Low Frequency Structures in the Wake of Elliptical Cylinders, *Eur. J. Mech. B/Fluids*, 23 (2004), 1, pp. 229-239
- [20] Yoon, H. S., et al., Characteristics of Flow and Heat Transfer Around a Circular Cylinder Near a Moving Wall in Wide Range of Low Reynolds Number, *International Journal of Heat and Mass Transfer*, 53 (2010), 23-24, pp. 5111-5120